

Galactic and cosmological fast radio bursts as scaled-up solar radio bursts

F. Y. Wang,^{1,2}* G. Q. Zhang,¹ Z. G. Dai^{1,2}

¹*School of Astronomy and Space Science, Nanjing University, Nanjing 210093, China*

²*Key Laboratory of Modern Astronomy and Astrophysics (Nanjing University), Ministry of Education, Nanjing 210093, China*

Accepted XXX. Received YYY; in original form ZZZ

ABSTRACT

Fast radio bursts (FRBs) are bright milliseconds radio transients with large dispersion measures. Recently, FRB 200428 was detected in temporal coincidence with a hard X-ray flare from the Galactic magnetar SGR 1935+2154, which supports that at least some FRBs are from magnetar activity. Interestingly, a portion of X-ray flares from magnetar XTE J1810-197 and the Sun are also accompanied by radio bursts. Many features of Galactic FRB 200428 and cosmological FRBs resemble solar radio bursts. However, a common physical origin among FRBs, magnetar radio pulses and solar radio bursts has not yet been established. Here we report a universal correlation between X-ray luminosity and radio luminosity over twenty orders of magnitude among solar type III radio bursts, XTE J1810-197 and Galactic FRB 200428. This universal correlation reveals that the energetic electrons which produce the X-ray flares and those which cause radio emissions have a common origin, which can give stringent limits on the generation process of radio bursts. Moreover, we find similar occurrence frequency distributions of energy, duration and waiting time for solar radio bursts, SGR 1935+2154 and repeating FRB 121102, which also support the tight correlation and the X-ray flares temporally associated with radio bursts. All of these distributions can be understood by avalanche models of self-organized criticality systems. The universal correlation and statistical similarities indicate that the Galactic FRB 200428 and FRBs seen at cosmological distances can be treated as scaled-up solar radio bursts.

Key words: Fast radio bursts

1 INTRODUCTION

Fast radio bursts (FRBs) are intense radio transients with extreme high brightness temperatures that show dispersion relations to be consistent with propagation through cold plasma (Lorimer et al. 2007; Thornton et al. 2013). Until now, more than one hundred FRBs have been discovered. All previous localized FRBs were at cosmological distances (Chatterjee et al. 2017; Bannister et al. 2019; Prochaska et al. 2019; Ravi et al. 2019; Marcote et al. 2020; Macquart et al. 2020). Even with precise localizations in their host galaxies, the physical origin of FRBs is still a mystery (Platts et al. 2019; Zhang 2020). Magnetars have been proposed as the possible engine to power repeating bursts from FRB sources (Popov & Postnov 2013; Kulkarni et al. 2014; Murase et al. 2016; Katz 2016; Metzger et al. 2017; Wang & Yu 2017; Beloborodov 2017; Yang & Zhang 2018; Wang et al. 2020).

The situation is dramatically changed with the recent discovery of FRB 200428 from the Galactic soft-gamma repeater (SGR) 1935+2154 independently by the Canadian Hydrogen Intensity Mapping Experiment (CHIME/FRB Collaboration et al. 2020) and the Survey for Transient Astronomical Radio Emission 2 (STARE2) (Bochenek et al. 2020). Meanwhile, a hard X-ray burst from SGR 1935+2154 was temporally coincident with this FRB, which has been observed by many telescopes (Li et al. 2020; Tavani et al. 2020; Ridnaia et al. 2020; Mereghetti et al. 2020). The fluence of this FRB at 1.4 GHz is 1.5 ± 0.3 Mega-Jy ms (Bochenek et al. 2020). This burst

is about a factor of 40 less energetic than the weakest burst detected from localized cosmological FRB sources, but a factor of 4×10^3 more energetic than any millisecond radio burst previously observed in the Milky Way. This discovery strongly supports the models based on magnetars that have been proposed for cosmological FRBs, and also proves the physical connection between X-ray bursts and radio bursts. Only a small fraction of X-ray flares is accompanied by luminous FRBs, based on the fact that 29 of the X-ray flares from SGR 1935+2154 have no radio signal detected down to mJy ms by Five-hundred-meter Aperture Spherical radio Telescope (Lin et al. 2020). Recently, bright X-ray pulses in temporal coincidence with radio pulses were detected from Galactic magnetar XTE J1810-197 (Pearlman et al. 2020). Although the radio pulses have lower energies compared with FRBs, they have similar characteristics to radio bursts detected from FRBs, such as millisecond duration and frequency structure. This suggests active magnetars can generate radio and X-ray emissions in a large energy range.

On the other hand, it is well known that solar type III radio bursts are usually associated with solar X-ray flares (Bastian et al. 1998). Solar type III radio bursts, identified by high brightness temperatures and rapid frequency drift, are a common signature of fast electron beams generated during solar flares. They are produced by coherent emissions arising from the nonlinear conversion of Langmuir waves generated by two-stream instability of electron beams (Ginzburg & Zhelezniakov 1958; Melrose 2017). Observations show that about 30% hard X-ray flares are temporally correlated with type III radio bursts (Reid & Vilmer 2017). There are at least four common properties for FRBs and solar type III radio bursts. First, they both have high

* E-mail: fayinwang@nju.edu.cn

brightness temperatures, 10^6 K- 10^{12} K for solar radio bursts and as high as 10^{35} K for FRBs. Second, the frequency drift (high-to-low temporal evolution) is found in repeating FRBs (Hessels et al. 2019), and solar type III radio bursts. Third, both radio bursts show similar intensity temporal evolution (Bastian et al. 1998; Hessels et al. 2019). Fourth, both radio bursts have been found to be temporally correlated with X-ray flares. Lyutikov (2002) already proposed that magnetar radio/X-ray flares are similar to solar flares, triggered by the magnetic field instabilities in the magnetars' magnetospheres. In this model, because the radio emission is generated by the electrons accelerated at the reconnection site, the intensity and profile of radio bursts will be strongly correlated with the X-ray bursts, which is confirmed by the two peaks of FRB 200428 and the associated X-ray flare peaks.

Although radio bursts are common phenomena in FRB sources, magnetars and the Sun, the burst luminosity spans more than 20 orders of magnitude. They also show similar features. However, a physical analogy among FRBs, magnetar radio pulses and solar type III radio bursts has not yet been established. It is generally accepted that the energetic electrons which produce the hard X-ray flares and those which cause the type III radio emissions during a solar flare have a common origin, which indicates that the X-ray flare emissions are correlated with the radio burst emissions (Bastian et al. 1998). Whether this correlation exists in magnetars and FRB sources is unclear.

Power-law size distributions are found in many astrophysical systems (for a review, see Aschwanden et al. 2016). Solar X-ray flares have been found to show power-law size distributions (Crosby et al. 1993). Giant pulses of several pulsars show power-law size distributions (Cognard et al. 1996; Lundgren et al. 1995; Cairns 2004). The size distributions of the fluences of SGR 1900+14 and SGR 1806-20 are found to exhibit power-law distributions with slopes around $\alpha_E \sim 1.6$ (Göğüş et al. 1999; Göğüş et al. 2000). So it is urgent to know whether FRBs and the associated X-ray bursts of magnetars show similar size distributions.

In this paper, we will show that the three kinds of radio bursts and the accompanied X-ray flares follow a universal correlation between X-ray luminosity L_X and radio luminosity L_R . Moreover, the radio bursts and the accompanied X-ray flares of FRB sources and the Sun show similar energy, duration and waiting time distributions. The structure of this paper is arranged as follows. In next section, the data sample are given. In section 3, we show the results. Summary is given in section 5.

2 DATA SAMPLE

2.1 Data used in $L_X - L_R$ correlation

The detection by CHIME in 400-800 MHz band reveals that FRB 200428 has two pulses, each about 0.5 ms wide and separated by 28.91 ms (CHIME/FRB Collaboration et al. 2020). So the duration is about 30 ms. The peak flux densities for the two peaks are 110 kJy and 150 kJy (CHIME/FRB Collaboration et al. 2020), respectively. The observation by STARE2 shows that the peak fluence in the 1281-1468 MHz is 1.5 ± 0.3 MJy ms (Bochenek et al. 2020). The flux difference may be due to the complex spectral feature. Because the two bands are very close, we adopt the peak fluence from STARE2 and the duration from CHIME. The peak radio luminosity is 2.61×10^{27} erg s^{-1} Hz $^{-1}$. The associated X-ray flare has a peak flux of 6×10^{-6} erg cm^{-2} s^{-1} in 20-200 keV band (Mereghetti et al. 2020). The distance to SGR 1935+2154 can range from 6.6 kpc to 12.5 kpc (Kothes et al. 2018; Zhou et al. 2020; Zhong et al. 2020). In this paper, 6.6 ± 0.7

kpc is used (Zhou et al. 2020). The peak luminosity for the X-ray flare is 3.13×10^{40} erg s^{-1} .

We also used the fluxes of type III radio bursts and X-ray flares given by Reid & Vilmer (2017) (Reid & Vilmer 2017). The 164 MHz flux for radio bursts and 25-50 keV flux for X-ray flares are selected, where the peaks in the two bands must be within 40 s of each other. Because the radio luminosity at 1.4 GHz of FRB 200428 is used, the 164 MHz flux is scaled to 1.4 GHz by assuming a spectral index of -1.78 (Reid & Vilmer 2017). When calculating the X-ray flux, the spectrum $dN/dE \propto E^{-3.9}$ at 25-50 keV is used (Benz & Güdel 2010).

XTE J1810-197 was discovered by the Rossi X-ray Timing Explorer in 2003 (Ibrahim et al. 2004). The distance to this magnetar is about 4 kpc (Minter et al. 2008). Recently, simultaneous radio pulses by NASA DSN 34m radio telescopes and X-ray pulses by Neutron star Interior Composition Explorer (NICER) are detected from XTE J1810-197 (Pearlman et al. 2020). The observational bands are 4.8 GHz and 0.5-10 keV for radio and X-ray, respectively. We use the parameters of radio and X-ray bursts shown in figure 2 of Pearlman et al. (2020). The number of bursts is 19. The area of NICER X-ray Timing Instrument is 1900 cm^2 . The spectral index is from -0.5 to 0 between 1.4 and 144 GHz (Pearlman et al. 2020). In calculation, we assume a flat spectrum to obtain the radio flux density at 1.4 GHz. The radio pulses from XTE J1810-197 share similarities with the radio bursts from repeating FRB sources, such as millisecond duration, frequency structure and narrow emission range. It must be noted that the X-ray pulses from XTE J1810-197 are temporally distinct and less energetic than giant flares and X-ray bursts previously observed from magnetars (Pearlman et al. 2020), indicating that they display highly variable X-ray emission. But the processes responsible for this behavior remain a mystery, which encourages us to build a unified picture. The X-ray band is different from that of SGR 1935+2154 flare. According to the X-ray burst of XTE J1810-197 observed in 2018, the luminosity in 2-10 keV band is comparable to that in the high-energy band (Gotthelf et al. 2019). Therefore, we assume that the luminosity in 2-10 keV band is similar as the high-energy one.

2.2 Data used in frequency distributions

The FRB 121102 has the largest burst sample. We collect the bursts of FRB 121102 from the observation by Green Bank telescope at 4-8 GHz. Recent work identified 93 pulses of FRB 121102 from 6 hours of observation (Gajjar et al. 2018; Zhang et al. 2018). This observation constructs the largest sample of FRB 121102 for a single observation. Using this sample, we can avoid the complex selection effect caused by the different telescopes at different frequencies.

For SGR 1935+2154, the bursts observed by Gamma-ray Burst Monitor on the Fermi Gamma-ray Space Telescope from 2014 to 2016 are used (Lin et al. 2020). The number of bursts is 112.

As for solar type III radio bursts, we select the data from the National Centers for Environmental Information (NCEI) observed by United States Air Force Radio Solar Telescope Network (RSTN)¹, which has observed for many years and has accumulated lots of data. RSTN consists of four sites: Learmonth, Palehua, Sagamore Hill and San Vito. The device and analysis methods in all sites are identical, so we can simply put them together to study their statistical properties. The data of RSTN contains solar radio bursts at 8 frequencies (245 MHz, 410 MHz, 610 MHz, 1415 MHz, 2695 MHz, 4995 MHz, 8800

¹ <ftp://ftp.ngdc.noaa.gov/STP/space-weather/solar-data/solar-features/solar-radio/radio-bursts/reports/fixd-frequency-listings/>

MHz, 15400 MHz). We divide the data into multiple subsamples based on frequency and calculate their statistical nature on each frequency. In order to obtain high quality data, we filter the data according to the criteria of Giersch et al. (2017). Based on these criteria, we select a large sample of solar type III radio bursts. The data of RSTN consists of eight frequencies. In these frequencies, 4995 MHz is more interesting, because it has the similar frequency with the data of FRB 121102. We also found that the best-fitting parameters ($\alpha_E, \alpha_T, \lambda_0$) are consistent with each other for the eight frequencies.

3 RESULTS

3.1 A universal correlation between X-ray and radio luminosities

Figure 1 shows the correlation between peak X-ray luminosity (L_X in units of ergs per second) and simultaneously peak radio luminosity (L_R in units of ergs per second per hertz) for solar type III radio bursts, magnetar XTE J1810-197 (Pearlman et al. 2020) and FRB 200428 (Bochenek et al. 2020; Mereghetti et al. 2020). Fitting the solar and XTE J1810-197 data, a tight correlation

$$\log L_X = (1.10 \pm 0.01) \times \log L_R + (10.17 \pm 0.10) \quad (1)$$

with a linear regression coefficient R-square=0.993 is found. The data of FRB 200428 (red square) is dramatically consistent with this correlation. The similarity of the luminosity ratio L_X/L_R , over twenty orders of magnitude in luminosity is surprising. The correlation suggests that the energetic electrons which produce the hard X-ray flares and those which generate radio emissions have a common origin. This $L_X - L_R$ correlation can be used to test the nature of a phenomenon and the mechanism of the associated radio emission. Some theoretical models also predict larger X-ray flares accompanying brighter FRBs (Metzger et al. 2019; Lyutikov & Popov 2020; Lu et al. 2020). This correlation can be tested with future simultaneous observations of FRBs and X-ray flares from magnetars. The dashed line in figure 1 shows the Güdel-Benz correlation between L_X and L_R (Guedel & Benz 1993), which only holds for gyrosynchrotron radio emissions and thermal X-ray emissions. For solar type III radio bursts, magnetar radio pulses and FRBs, the radio emissions are coherent emission, not gyrosynchrotron radiation. Therefore, they deviate from the Güdel-Benz correlation.

3.2 Occurrence frequency distributions

Below, we discuss the frequency distributions of solar type III radio bursts, SGR 1935+2154 and FRB 121102, inspired by the fact that solar radio bursts and FRB 200428 are both associated with X-ray flares. The tight correlation and X-ray flares temporally associated with radio bursts also require the occurrence frequency distributions of energy, duration and waiting time for them are similar.

Figure 2 shows the energy frequency distributions of solar type III radio bursts, SGR 1935+2154 and FRB 121102. For solar radio bursts, the differential distribution is used. The number of bursts $N(E)dE$ with energy between E and $E + dE$ can be expressed by

$$dN/dE \propto E^{-\alpha_E}, \quad (2)$$

where α_E is the power-law index. The numbers of bursts of FRB 121102 and SGR 1935+2154 are small, so it's preferable to consider cumulative distribution (Aschwanden 2015)

$$N(> E) = 1 + (N_{ev} - 1) \left(\frac{(E_2 + E_0)^{1-\alpha_E} - (E + E_0)^{1-\alpha_E}}{(E_2 + E_0)^{1-\alpha_E} - (E_1 + E_0)^{1-\alpha_E}} \right) \quad (3)$$

rather than the differential distribution. In the above equation, N_{ev} is the number of bursts, E_0 is a threshold value, α is the power-law index, E_1 and E_2 is the minimum energy and maximum energy, respectively. We use the uniform logarithmic bins to group these bursts and the error of i th bin is $\sqrt{N_i - N_{i+1}}$, where N_i and N_{i+1} is the number of bursts in each bin (Aschwanden 2019). This method takes only independent events into account for the estimation of the uncertainty. The Markov chain Monte Carlo (MCMC) technique is used to derive the best-fitting parameters. The best-fitting power-law indices are $\alpha_E = 1.51 \pm 0.19, 1.66 \pm 0.06$ and 1.82 ± 0.20 for solar radio bursts, FRB 121102 and SGR 1935+2154 with 1σ errors, respectively. The energy distributions for the three sources are consistent with each other at 1σ confidence level. The energy distribution of solar radio bursts is consistent with that of type III radio bursts observed by the Nancay Radioheliograph from 1998 to 2008 (Saint-Hilaire et al. 2013). The value of α_E for SGR 1935+2154 is consistent with other SGRs (Cheng et al. 2020). However, a slight larger value of $\alpha_E = 1.78 \pm 0.01$ is found by Lin et al. (2020) using an ideal power-law function. The reason is that the high-energy cutoff is considered in our fitting. Yang et al. (2020) also found the power-law index is $\alpha_E = 1.72^{+0.13}_{-0.19}$ at high-energy range. The similar power-law indices between SGR 1935+2154 and FRB 121102 support that the tight correlation between radio burst luminosity and X-ray flare luminosity. We also try to use the broken power-law function to fit the energy distribution of FRB 121102. The fitting result is shown as red dashed line in Figure 2. The power-law index for the low energy band is $\alpha_{E,low} = 1.75 \pm 0.64$ and that of high energy end is $\alpha_{E,high} = 2.38 \pm 0.51$. The fit of broken power-law looks much better. But given the small number of bursts, the error of the fitting results are large. The steepness of power-law slope may be associated with finite-size effects in a self-organized criticality (SOC) system, which can cause an exponential-like cutoff at the upper end of the size distribution, as it is found in many astrophysical systems (Aschwanden et al. 2016).

Figure 3 shows the differential distribution of duration T for solar type III radio bursts at 4995 MHz (left panel), the cumulative distributions of duration for FRB 121102 (middle panel) and SGR 1935+2154 (right panel), respectively. Using the same fitting method as Figure 2, we find the power-law indices are $\alpha_T = 1.69 \pm 0.02, 1.57 \pm 0.11$ and 1.78 ± 0.06 for solar radio bursts, FRB 121102 and SGR 1935+2154, respectively. The value of α_T for SGR 1935+2154 is consistent with those of other SGRs (Wang & Yu 2017). We can see that the duration distributions for the three sources are consistent with each other at 1σ confidence level. The broken power-law function is also used to fit the duration distribution of SGR 1935+2154. We show the results in Figure 3 with red dashed line. The index of low-energy band is $\alpha_{T,low} = 1.62 \pm 0.54$, which is consistent with that of single power-law fit. The index of high-energy end is $\alpha_{T,high} = 2.69 \pm 0.24$.

From Figures 2 and 3, we have found a similar power-law dependence of the occurrence rate (energy and duration) for solar radio bursts, FRB 121102 and SGR 1935+2154. Interestingly, solar X-ray flares in temporal with solar type III radio bursts also show a similar power-law distribution (Crosby et al. 1993; Wang & Dai 2013). These distributions can be well understood within the statistical framework of a self-organized criticality (SOC) system (Katz 1986; Bak et al. 1987; Lu & Hamilton 1991). The power-law distributions of energy and duration naturally follow from such a model since the system has no characteristic spatial scale above the elementary scale of the smallest avalanche (the smallest-energy event), up to the system size. The power-law indices are consistent with the prediction of the fractal-diffusive SOC model in 3-dimension Euclidean space (Aschwanden

2012). Interestingly, similar dimension was also found in the pulses of prompt emission of gamma-ray bursts (Lyu et al. 2020).

What can we learn from the similar distributions between solar type III radio bursts and FRBs? It is generally believed that type III bursts arise from the nonlinear conversion of Langmuir waves at the local plasma frequency by energetic electron beams accelerated during solar flares (Ginzburg & Zhelezniakov 1958). Numerical simulations have revealed that solar radio bursts are caused by particle acceleration episodes that result from bursty magnetic reconnection. From observations, direct evidences have been found that energetic electrons are accelerated by magnetic reconnections, which also produce X-ray flares (Cairns et al. 2018). The similar energy and duration distributions support that both radio bursts and associated X-ray flares are triggered by magnetic reconnection as speculated by some theoretical models (Lyutikov 2002; Katz 2016; Lyutikov & Popov 2020). The similar power-law distributions of solar radio bursts and hard X-ray flares, together with similar power-law distributions between SGR X-ray flares and FRBs, strengthens the fact that X-ray and radio emissions are tightly correlated in these sources.

The third statistical property is the waiting time distribution, which has been well studied in solar X-ray flares (Wheatland et al. 1998), and X-ray flares in gamma-ray bursts (Wang & Dai 2013). The waiting time Δt is defined as the time interval between two successive bursts. This distribution provides extra constraints on theoretical models. For example, avalanche models predict that bursts occur independently (Wheatland et al. 1998). We use Poisson process to explain the waiting time distributions. For constant burst rate, the waiting time follows the Poisson interval distribution (Wheatland et al. 1998)

$$P(\Delta t) = \lambda e^{-\lambda \Delta t}, \quad (4)$$

where λ is the burst rate. If the rate is time dependent, the distribution can be treated as a piecewise constant Poisson process consisting N intervals with λ_i and duration t_i . The wait time distribution can be derived by (Aschwanden & McTiernan 2010)

$$P(\Delta t) \approx \frac{1}{\bar{\lambda}} \sum_{i=1}^N \frac{t_i}{T} \lambda_i^2 e^{-\lambda_i \Delta t}, \quad (5)$$

where $\bar{\lambda}$ is the average burst rate and T is the duration of the observing period (Wheatland et al. 1998). Equation (5) can be transformed into a continuous function

$$P(\Delta t) = \frac{\int_0^T \lambda(t)^2 e^{-\lambda(t)\Delta t} dt}{\int_0^T \lambda(t) dt}. \quad (6)$$

For the exponentially growing occurrence rate $f(\lambda) = \lambda^{-1} \exp(-\lambda/\lambda_0)$ (Aschwanden & McTiernan 2010), the waiting time distribution is

$$P(\Delta t) = \frac{\lambda_0}{(1 + \lambda_0 \Delta t)^2}. \quad (7)$$

For large waiting times ($\Delta t \gg 1/\lambda_0$), it gives the power-law limit $P(\Delta t) \approx \Delta t^{-2}$.

Figure 4 shows the occurrence rates as a function of waiting times for solar type III radio bursts at 4995 MHz (left panel), FRB 121102 (middle panel) and SGR 1935+2154 (right panel), respectively. The fitting results from MCMC method using equation (7) are shown as solid lines in Figure 4. The mean rates are $\lambda_0 = 1.10^{+0.06}_{-0.05} \times 10^{-5} (6s)^{-1}$, $1.37^{+0.34}_{-0.26} \times 10^{-5} \text{ ms}^{-1}$ and $22.78^{+2.41}_{-2.30} \text{ day}^{-1}$ for solar radio bursts, FRB 121102 and SGR 1935+2154, respectively. The waiting times in these sources can be understood by the same exponentially growing occurrence model. The best-fitting parameters are shown in Table 1. The same waiting

time distributions of SGR 1935+2154 and FRB 121102 also support the tight correlation between radio and X-ray emissions. The difference of mean rate λ_0 indicates that the magnetar powered FRB 121102 is much more active than SGR 1935-2154. The central magnetar of FRB 121102 is estimated to be very young, about a few decades (Metzger et al. 2017; Cao et al. 2017; Zhao et al. 2020). The age of SGR 1935+2154 is uncertain, from 3000 years (Israel et al. 2016), to 16000 years (Zhou et al. 2020). According to Beloborodov & Li (2016), the magnetic activity timescale is about 20 years in the direct Urca case (high-mass neutron star) and 700 years in modified Urca (normal-mass neutron star) case. Therefore, the mean rate of FRB 121102 is higher than that of SGR 1935+2154.

4 SUMMARY

Many similar phenomena occur in astrophysical systems with spatial and magnetic field scales different by many orders of magnitudes. In this paper, based on the observational facts that the radio bursts in the Sun, XTE J1810-197 and FRB 200428 are all accompanied by X-ray flare emissions, we find a universal correlation $\log L_X = (1.12 \pm 0.02) \times \log L_R + 10.22 \pm 0.26$ between X-ray luminosity and radio luminosity over twenty orders of magnitude in these sources. This correlation implies that the energetic electrons producing the X-ray flares and those causing the radio emissions have a common origin. It must be noted that in the Güdel-Benz correlation, the radio emissions are gyrosynchrotron radiation. However, the radio emission is from coherent process in our correlation. In future, this correlation can be tested using more FRBs and associated X-ray flares. For solar flares, the arrive time of radio peak is delayed by about a few seconds relative to the hard X-ray flare peak (Bastian et al. 1998). For FRB 200428, the two X-ray peaks occur within about $t_\delta \sim 3$ ms of the corresponding radio burst peaks (CHIME/FRB Collaboration et al. 2020; Li et al. 2020). Therefore, high-time resolution observations are needed to clarify this point (Mereghetti et al. 2020; Margalit et al. 2020; Wu et al. 2020). The time delay is also important to distinguish physical models (Lyutikov & Popov 2020; Metzger et al. 2019).

We also found similar statistical properties, including power-law distributions of energy, duration and waiting time, among solar radio bursts, FRB 121102 and SGR 1935-2154. The universal $L_X - L_R$ correlation is also supported by the same energy and waiting time distributions of SGR 1935-2154 and FRB 121102. The radio bursts and X-ray flares in the Sun and magnetar SGR 1935+2154 are both show similar power-law distributions. These distributions can be well understood within the statistical framework of a self-organized criticality system. The universal correlation and the statistical similarities, together with the fact that solar radio bursts and X-ray flares are powered by magnetic energy, reveal that Galactic and cosmological FRBs are powered by magnetic energy of magnetars, and can be treated as scaled-up solar radio bursts. It supports that magnetic activities govern the fundamental physical processes in all of these systems. It must be noted that magnetars differ from solar radio sources in their many orders of magnitude higher rotation rate, which creates much different electro-dynamic and magneto-hydrodynamic effects (e.g., Sturrock & Aschwanden 2012), which should be extensively studied.

ACKNOWLEDGEMENTS

We thank the anonymous referee for constructive and helpful comments. This work is supported by the National Natural Science Foundation of China (grants U1831207 and 11833003), and the

National Key Research and Development Program of China (grant 2017YFA0402600).

DATA AVAILABILITY

The data used in the paper is included in the published papers as shown in Section 2.

REFERENCES

- Aschwanden M. J., 2012, *A&A*, **539**, A2
 Aschwanden M. J., 2015, *ApJ*, **814**, 19
 Aschwanden M. J., 2019, *ApJ*, **880**, 105
 Aschwanden M. J., McTiernan J. M., 2010, *ApJ*, **717**, 683
 Aschwanden M. J., et al., 2016, *Space Sci. Rev.*, **198**, 47
 Bak P., Tang C., Wiesenfeld K., 1987, *Phys. Rev. Lett.*, **59**, 381
 Bannister K. W., et al., 2019, *Science*, **365**, 565
 Bastian T. S., Benz A. O., Gary D. E., 1998, *ARA&A*, **36**, 131
 Beloborodov A. M., 2017, *ApJ*, **843**, L26
 Beloborodov A. M., Li X., 2016, *ApJ*, **833**, 261
 Benz A. O., Güdel M., 2010, *ARA&A*, **48**, 241
 Bochenek C. D., Ravi V., Belov K. V., Hallinan G., Kocz J., Kulkarni S. R., McKenna D. L., 2020, *Nature*, **587**, 59
 CHIME/FRB Collaboration Andersen B. C., et al., 2020, *Nature*, **587**, 54
 Cairns I. H., 2004, *ApJ*, **610**, 948
 Cairns I. H., et al., 2018, *Scientific Reports*, **8**, 1676
 Cao X.-F., Yu Y.-W., Dai Z.-G., 2017, *ApJ*, **839**, L20
 Chatterjee S., et al., 2017, *Nature*, **541**, 58
 Cheng Y., Zhang G. Q., Wang F. Y., 2020, *MNRAS*, **491**, 1498
 Cognard I., Shrauner J. A., Taylor J. H., Thorsett S. E., 1996, *ApJ*, **457**, L81
 Crosby N. B., Aschwanden M. J., Dennis B. R., 1993, *Sol. Phys.*, **143**, 275
 Gajjar V., et al., 2018, *ApJ*, **863**, 2
 Giersch O. D., Kennewell J., Lynch M., 2017, *Space Weather*, **15**, 1511
 Ginzburg V. L., Zhelezniakov V. V., 1958, *Soviet Ast.*, **2**, 653
 Gotthelf E. V., et al., 2019, *ApJ*, **874**, L25
 Göğüş E., Woods P. M., Kouveliotou C., van Paradijs J., Briggs M. S., Duncan R. C., Thompson C., 1999, *ApJ*, **526**, L93
 Göğüş E., Woods P. M., Kouveliotou C., van Paradijs J., Briggs M. S., Duncan R. C., Thompson C., 2000, *ApJ*, **532**, L121
 Guedel M., Benz A. O., 1993, *ApJ*, **405**, L63
 Hessels J. W. T., et al., 2019, *ApJ*, **876**, L23
 Ibrahim A. I., et al., 2004, *ApJ*, **609**, L21
 Israel G. L., et al., 2016, *MNRAS*, **457**, 3448
 Katz J. I., 1986, *J. Geophys. Res.*, **91**, 10,412
 Katz J. I., 2016, *ApJ*, **826**, 226
 Kothes R., Sun X., Gaensler B., Reich W., 2018, *ApJ*, **852**, 54
 Kulkarni S. R., Ofek E. O., Neill J. D., Zheng Z., Juric M., 2014, *ApJ*, **797**, 70
 Li C. K., et al., 2020, arXiv e-prints, p. arXiv:2005.11071
 Lin L., et al., 2020, *Nature*, **587**, 63
 Lorimer D. R., Bailes M., McLaughlin M. A., Narkevic D. J., Crawford F., 2007, *Science*, **318**, 777
 Lu E. T., Hamilton R. J., 1991, *ApJ*, **380**, L89
 Lu W., Kumar P., Zhang B., 2020, *MNRAS*, **498**, 1397
 Lundgren S. C., Cordes J. M., Ulmer M., Matz S. M., Lomatch S., Foster R. S., Hankins T., 1995, *ApJ*, **453**, 433
 Lyu F., Li Y.-P., Hou S.-J., Wei J.-J., Geng J.-J., Wu X.-F., 2020, *Frontiers of Physics*, **16**, 14501
 Lyutikov M., 2002, *ApJ*, **580**, L65
 Lyutikov M., Popov S., 2020, arXiv e-prints, p. arXiv:2005.05093
 Macquart J. P., et al., 2020, *Nature*, **581**, 391
 Marcote B., et al., 2020, *Nature*, **577**, 190
 Margalit B., Beniamini P., Sridhar N., Metzger B. D., 2020, *ApJ*, **899**, L27
 Melrose D. B., 2017, *Reviews of Modern Plasma Physics*, **1**, 5
 Mereghetti S., et al., 2020, *ApJ*, **898**, L29
 Metzger B. D., Berger E., Margalit B., 2017, *ApJ*, **841**, 14
 Metzger B. D., Margalit B., Sironi L., 2019, *MNRAS*, **485**, 4091
 Minter A. H., Camilo F., Ransom S. M., Halpern J. P., Zimmerman N., 2008, *ApJ*, **676**, 1189
 Murase K., Kashiyama K., Mészáros P., 2016, *MNRAS*, **461**, 1498
 Pearlman A. B., et al., 2020, arXiv e-prints, p. arXiv:2005.08410
 Platts E., Weltman A., Walters A., Tendulkar S. P., Gordin J. E. B., Kandhai S., 2019, *Phys. Rep.*, **821**, 1
 Popov S. B., Postnov K. A., 2013, arXiv e-prints, p. arXiv:1307.4924
 Prochaska J. X., et al., 2019, *Science*, **366**, 231
 Ravi V., et al., 2019, *Nature*, **572**, 352
 Reid H. A. S., Vilmer N., 2017, *A&A*, **597**, A77
 Ridnaia A., et al., 2020, arXiv e-prints, p. arXiv:2005.11178
 Saint-Hilaire P., Vilmer N., Kerdraon A., 2013, *ApJ*, **762**, 60
 Sturrock P., Aschwanden M. J., 2012, *ApJ*, **751**, L32
 Tavani M., et al., 2020, arXiv e-prints, p. arXiv:2005.12164
 Thornton D., et al., 2013, *Science*, **341**, 53
 Wang F. Y., Dai Z. G., 2013, *Nature Physics*, **9**, 465
 Wang F. Y., Yu H., 2017, *J. Cosmology Astropart. Phys.*, **03**, 023
 Wang F. Y., Wang Y. Y., Yang Y.-P., Yu Y. W., Zuo Z. Y., Dai Z. G., 2020, *ApJ*, **891**, 72
 Wheatland M. S., Sturrock P. A., McTiernan J. M., 1998, *ApJ*, **509**, 448
 Wu Q., Zhang G. Q., Wang F. Y., Dai Z. G., 2020, *ApJ*, **900**, L26
 Yang Y.-P., Zhang B., 2018, *ApJ*, **868**, 31
 Yang Y.-P., Zhu J.-P., Zhang B., Wu X.-F., 2020, *ApJ*, **901**, L13
 Zhang B., 2020, *Nature*, **587**, 45
 Zhang Y. G., Gajjar V., Foster G., Siemion A., Cordes J., Law C., Wang Y., 2018, *ApJ*, **866**, 149
 Zhao Z. Y., Zhang G. Q., Wang Y. Y., Wang F. Y., 2020, arXiv e-prints, p. arXiv:2010.10702
 Zhong S.-Q., Dai Z.-G., Zhang H.-M., Deng C.-M., 2020, *ApJ*, **898**, L5
 Zhou P., Zhou X., Chen Y., Wang J.-S., Vink J., Wang Y., 2020, arXiv e-prints, p. arXiv:2005.03517

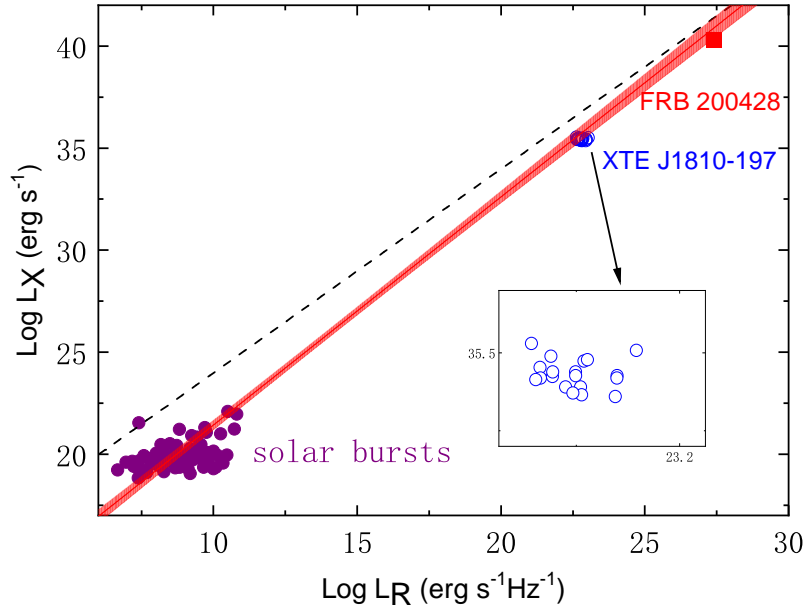


Figure 1. The $L_X - L_R$ correlation over twenty orders of magnitude. Purple points indicate solar type III radio bursts. X-ray and radio bursts from XTE J1810-197 are shown as blue open points. Red square shows the Galactic FRB 200428 and the associated X-ray flare. The red line is the fitting curve $\log L_X = (1.10 \pm 0.01) \times \log L_R + (10.17 \pm 0.10)$ (equation 1). FRB 200428 (red square) is dramatically consistent with this correlation. The dashed line is the Güdel-Benz correlation, which only can be used for gyrosynchrotron radio emissions. Apparently, the coherent radio emissions deviate from the Güdel-Benz correlation.

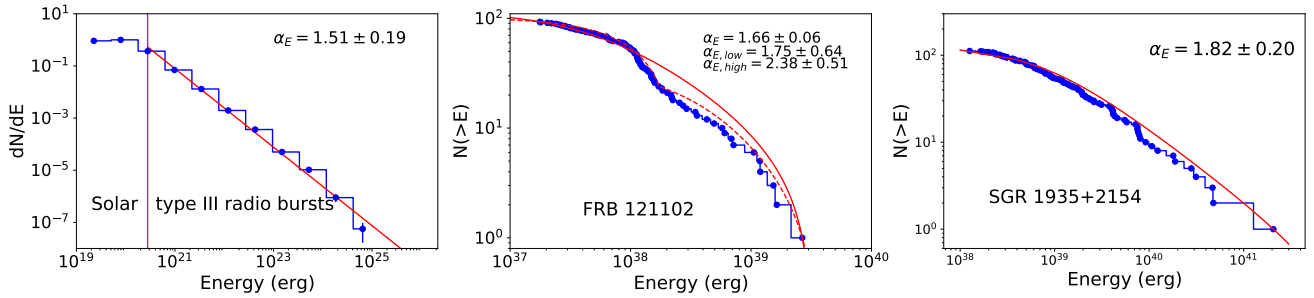


Figure 2. The occurrence frequency distribution of Energy. Error bars correspond to 68% Poisson confidence intervals for the event numbers. Left panel: the differential distribution of energy for solar type III radio bursts is shown as step-wise blue curve. The data is observed by the United States Air Force Radio Solar Telescope Network (RSTN) from the National Centers for Environmental information (NCEI) between 1979 and 2010. The best-fitting is shown as red line with power-law index $\alpha_E = 1.51 \pm 0.19$ (1σ). Middle panel: The step-wise blue curve represents the cumulative distribution of energy for FRB 121102. We fit the cumulative distribution using a power-law function with a threshold $N(>E) = 1 + (N_{ev} - 1) \left(\frac{(E_2 + E_0)^{1-\alpha_E} - (E + E_0)^{1-\alpha_E}}{(E_2 + E_0)^{1-\alpha_E} - (E_1 + E_0)^{1-\alpha_E}} \right)$ with $\alpha_E = 1.66 \pm 0.06$, which is shown as red line. We also show the fitting result of broken power-law in this panel with red dashed line. The power-law indices are also shown in this panel. Right panel: The cumulative distribution of energy for SGR 1935+2154 with the best-fitting $\alpha_E = 1.82 \pm 0.20$. In order to avoid the selection effect, only the data above the break (vertical line) is fitted. The power-law indices are consistent with each other at 1σ confidence level.

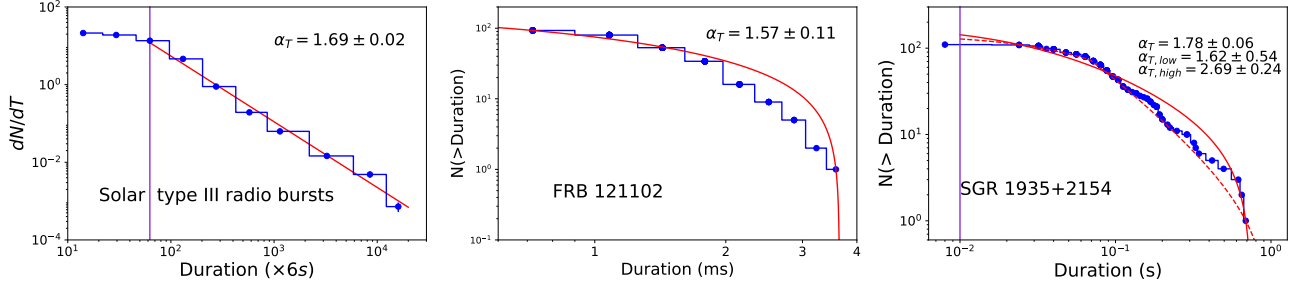


Figure 3. The frequency distribution of burst duration time. Left panel: we give the differential distribution of duration of solar type III radio bursts. The best fitting is $\alpha_T = 1.69 \pm 0.02$. Middle panel: The cumulative distribution of duration of FRB 121102 is shown. The best fitting is $\alpha_T = 1.57 \pm 0.11$ (red line). Right panel: The cumulative distribution of duration of SGR 1935+2154 is shown with the best-fitting $\alpha_T = 1.78 \pm 0.06$. In order to avoid the selection effect, only the data above the break (vertical line) is fitted. The red dashed line is the fitting result of broken power-law model. We show the power-law indices in this panel. Considering the 1σ uncertainties, the power-law indices are consistent.

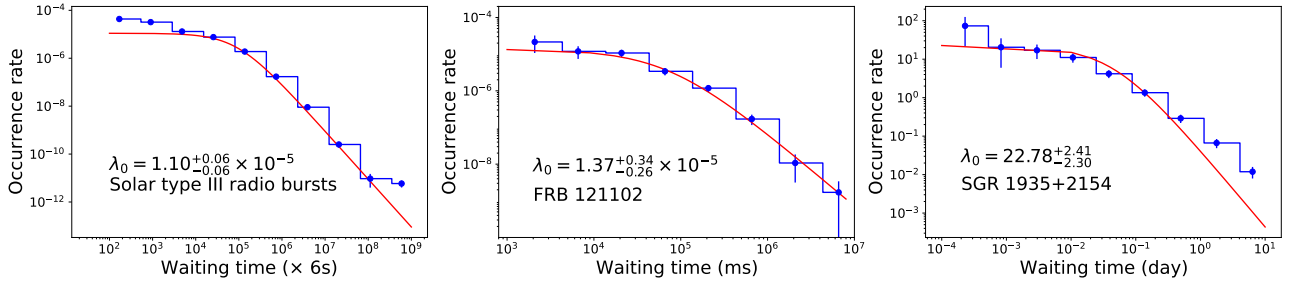


Figure 4. Waiting-time frequency distribution. Considering Poisson random process, we use $P(\Delta t) = \lambda_0 / (1 + \lambda_0 \Delta t)^2$ to fit the distributions. Left panel: The occurrence rate as a function of waiting time for solar type III radio bursts is shown as red line with best-fitting parameter $\lambda_0 = 1.10^{+0.06}_{-0.06} \times 10^{-5} (6s)^{-1}$. Middle panel: The occurrence rate as a function of waiting time for FRB 121102. The best-fitting parameter is $\lambda_0 = 1.37^{+0.34}_{-0.26} \times 10^{-5} ms^{-1}$. Right panel: The occurrence rate as a function of waiting time for SGR 1935+2154. The best-fitting parameter is $\lambda_0 = 22.78^{+2.41}_{-2.30} day^{-1}$. The waiting time distributions in these three sources can be explained by the same exponentially growing occurrence model.

Table 1. The fitting results for solar radio bursts, FRB 121102 and SGR 1935+2154 with equation (3). The uncertainties are the 68.3% confidence interval.

source	number of bursts	α_E	α_T	λ_0
solar radio bursts	2091	1.51 ± 0.19	1.69 ± 0.02	$1.10^{+0.06}_{-0.06} \times 10^{-5} (6s)^{-1}$
FRB 121102	93	1.66 ± 0.06	1.57 ± 0.11	$1.37^{+0.34}_{-0.26} \times 10^{-5} ms^{-1}$
SGR 1935+2154	112	1.82 ± 0.20	1.78 ± 0.06	$22.78^{+2.41}_{-2.30} day^{-1}$